

Self-organization of spatio-temporal earthquake clusters

S. Hainzl, G. Zöller and J. Kurths

Institute of Physics, University of Potsdam, D-14469 Potsdam, Germany

Received: 20 January 1998 – Accepted: 17 March 2000

Abstract. Cellular automaton versions of the Burridge-Knopoff model have been shown to reproduce the power law distribution of event sizes; that is, the Gutenberg-Richter law. However, they have failed to reproduce the occurrence of foreshock and aftershock sequences correlated with large earthquakes. We show that in the case of partial stress recovery due to transient creep occurring subsequently to earthquakes in the crust, such spring-block systems self-organize into a statistically stationary state characterized by a power law distribution of fracture sizes as well as by foreshocks and aftershocks accompanying large events. In particular, the increase of foreshock and the decrease of aftershock activity can be described by, aside from a prefactor, the same Omori law. The exponent of the Omori law depends on the relaxation time and on the spatial scale of transient creep. Further investigations concerning the number of aftershocks, the temporal variation of aftershock magnitudes, and the waiting time distribution support the conclusion that this model, even “more realistic” physics is missed, captures in some ways the origin of the size distribution as well as spatio-temporal clustering of earthquakes.

1 Introduction

The dynamics of earthquakes has attracted much attention as a real-world example for a self-organized critical phenomenon, introduced by Bak et al. (1987). The hallmarks of systems exhibiting self-organized criticality (SOC) are spatial and temporal correlation functions with power law behavior.

In fact, earthquakes show several types of power law behavior. In particular, their frequency-size distribution is well defined by the Gutenberg-Richter law (Gutenberg and Richter, 1954)

$$\log_{10} N = a - b \cdot M, \quad (1)$$

Correspondence to: S. Hainzl

where N is the number of earthquakes with magnitude greater than or equal to M . Considering the relation between the magnitude M and its source size S , i.e. $M \sim \log S$ (Kanamori and Anderson, 1975; Purcaru and Berckhemer, 1978), the Gutenberg-Richter law describes a power law for the number of observed earthquakes with sizes greater than S ,

$$N \sim S^{-B}. \quad (2)$$

The exponent B varies over a wide range of values for different faults, namely, between 0.80 and 1.05 (Ekström and Dziewonski, 1988; Pacheco et al., 1992).

The first generation of SOC earthquake models, derived from the sandpile model (Bak et al., 1987), implying a conservation law with regard to the internal coupling rules (Bak and Tang, 1989; Ito and Matsuzaki, 1990). They reproduce the power law size distribution, but the observed B value was found to be universal and too small.

On the other hand, a geophysically motivated fault model, which was proposed earlier by Burridge and Knopoff (1967) (hereinafter referred to as BK), has also been shown to reproduce the Gutenberg-Richter law. In this case, a fault is modeled as a spring-block system lying between two moving rigid tectonic plates. Several modifications of this model have been analyzed by different authors (e.g., Carlson and Langer, 1989a, b). In the quasi-static limit; that is, if instantaneous block slips are assumed (Nakanishi, 1990; Brown et al., 1991; Olami et al., 1992; Rundle and Klein, 1995), this spring-block model is very similar to the first generation of SOC models, differs only in a deterministic instead of a stochastic forcing and in its nonconservative characteristics which comes from a coupling by springs between the blocks within the fault plane and the tectonic plate. Olami et al. (1992) (hereinafter referred to as OFC) have shown that the proper B value and its empirically observed variability can be reproduced, if the level of conservation decreases in these cellular automaton versions of the BK

model. According to the OFC model, the exponent B is close to 0 in the case of high levels of conservation and increases to values above 2 for low levels of conservation.

However, all of these models fail to reproduce the spatio-temporal clustering of smaller events accompanying large earthquakes in real fault systems, namely the occurrence of foreshocks and aftershocks. On average, both the decay of aftershock sequences and the time distribution of foreshocks follow power laws. The aftershocks are described by the modified Omori law (Omori, 1894; Utsu et al., 1995)

$$R_a \sim (c_a + t - t_M)^{-p} \quad (3)$$

and the foreshocks by a similar power law, an inverse Omori law (Kagan and Knopoff, 1978; Jones and Molnar, 1979)

$$R_f \sim (c_f + t_M - t)^{-q}, \quad (4)$$

where t_M indicates the occurrence time of the mainshock; R_a and R_f denote the occurrence rate of aftershocks and foreshocks, respectively; and c_a , c_f are small constants scattering from 0.01 days to over 1 day with a median of about 0.3 days (Utsu et al., 1995). Both exponents p and q are found to be almost identical for empirical earthquake catalogs, whereas their value can vary between 0.9 and 1.5 (Papazachos, 1975; Utsu et al., 1995).

An aseismic phenomenon, which is correlated with large earthquakes in real fault systems, is postseismic creep. This transient process is observed to occur subsequently to earthquakes in the vicinity of the fault over days to years (Peltzer et al., 1996; Heki et al., 1997; Savage and Svarc, 1997). We have shown in previous investigations (Hainzl et al., 1999) that the introduction of postseismic transient creep characteristics in cellular automaton versions of the BK model leads to a reproduction of the empirically observed spatio-temporal earthquake clusters, especially to foreshock and aftershock sequences obeying the Omori law. In our previous work, the effect of stress recovery due to the transient creep was restricted only to the slipped block or to its four nearest neighbors neglecting more realistic long-range effects. Thus it is important to analyze the model results with regard to long-range interactions. This is the first aim of this paper. Furthermore, we give some more insights in the properties of the simulated spatio-temporal event clustering, especially concerning the aftershock sequences and the distribution of waiting times, and compare these results with empirical observations.

2 Model

Our aim is to characterize the qualitative behavior due to a time-dependent stress modulation subsequently to earthquakes. However, we do not want to model earthquake nucleation and rupture processes in detail. By

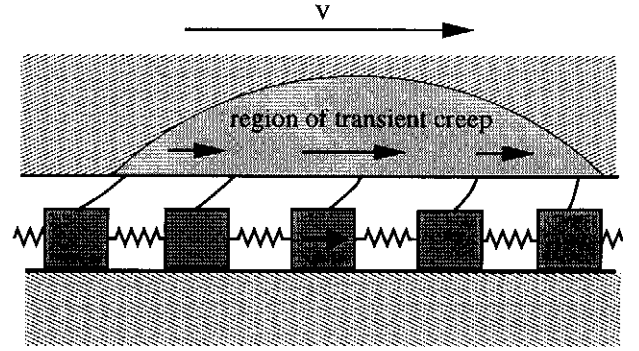


Fig. 1. One-dimensional sketch of the investigated two-dimensional spring-block model. The bottom blocks, which perform stick-slip motion, are connected to its neighbors by springs. Furthermore, each block is coupled by a loader spring to the upper tectonic plate moving with a velocity V and frictionally to the lower plate. The sliding of a block during an earthquake triggers subsequently transient creep within the tectonic plate, which leads locally to an increased loading after the earthquake.

analogy with the BK model, the fault is represented by a network of interconnected blocks lying between two tectonic plates. The blocks are driven by the slow relative movement of these two plates. Once the stress on a block exceeds the static friction, sliding is initiated and the frictional resistance of the block is assumed to drop instantaneously to the dynamic friction. The slip of the block redefines the stress of the blocks in the neighborhood. This can result in further slips and a chain reaction, i.e. an avalanche, can evolve, which is identified with an earthquake.

In contrast to the BK model and its cellular automaton version (OFC model), we do not assume total rigidity of the tectonic plates, because material creep, plasticity, fluid flow, and other processes are important in real fault systems. For example, afterslip or transient creep are known to induce a stress release in the order of the coseismic release (Heki et al., 1997; DeMets, 1997). Therefore we study, as an extension of the BK model, postseismic transient creep in the vicinity of the stucked fault layer blocks. A one-dimensional sketch of the investigated two-dimensional block system is shown in Figure 1. In general, a local failure changes the stress within the crust over a zone with a characteristic length set by the screening of the elastic Green function. Transient creep is expected to occur in this region. In previous investigations (Hainzl et al., 1999), we have restricted our analysis in a first-order approximation to transient creep that affects only the slipped block and its nearest neighbors. In this paper, we study alternatively long-range interactions. Thereby, the relaxation process of the crust is modeled by standard linear solids, which exhibit elastic properties in addition to transient creep characteristics. The response of a standard linear solid to an instantaneous stress change is described by a partial stress relaxation according to an exponential

function (see, e.g., Dieterich, 1972).

In real fault systems, the duration of large earthquakes is of the order of minutes, whereas the duration of aftershock sequences is of the order of weeks or months, and the recurrence times of large earthquakes are of the order of hundreds years. Consequently, the dynamics of a single earthquake are much faster than the assumed crust relaxation and tectonic loading. Therefore we assume that the crust relaxation and the tectonic loading have no effect on the dynamics of an individual event. Thus the evolution of a single earthquake depends only on the elastic properties of the block system and can be described by analogy with the OFC model. In the inter-occurrence time intervals between successive earthquakes, the stresses increase according to the tectonic loading and, additionally, in contrast to the OFC model, according to the transient creep in the crust.

We implement our model in the form of a continuous cellular automaton by defining an $L \times L$ array of blocks (i, j) , where i, j are integers, $1 \leq i, j \leq L$. The total force (or stress if unit area is assumed) on each block is given by $\sigma(i, j)$. The model algorithm consists of two steps, (1) the evolution of a single earthquake and (2) the stress changes in the inter-occurrence time between successive events.

1. The evolution of a single event is described in the following way: The friction law adopts the Mohr-Coulomb law with a spatially constant static failure threshold σ_F and residual stress σ_R . If the stress on a block (k, l) exceeds the static failure threshold, $\sigma(k, l) \geq \sigma_F$, sliding is initiated at this block. The moving block slips to the position with the residual stress σ_R , and the stress $\Delta\sigma \equiv \sigma(k, l) - \sigma_R$ is distributed to the adjacent blocks and to the crust. The stresses of the four nearest neighbors (k_{\pm}, l_{\pm}) are set according to the rule

$$\sigma(k_{\pm}, l_{\pm}) \rightarrow \sigma(k_{\pm}, l_{\pm}) + \alpha \Delta\sigma \quad (5)$$

and the stress of the sliding site is reset to

$$\sigma(k, l) \rightarrow \sigma_R. \quad (6)$$

The elastic coupling constant α depends on the spring constants and can vary in the range of $0 \leq \alpha \leq 0.25$, where $\alpha = 0.25$ refers to the conservative case (Olami et al., 1992; Hainzl et al., 1999). The block sliding leads to a reduced expansion of the loader spring, which connects the block with the tectonic plate; that is, to a reduced resistance force of the fault layer in this region $(1 - 4\alpha)\Delta\sigma$. This stress change is assumed to cause the relaxation process within the crust following subsequently to the earthquake (step 2). We introduce the stress levels $\sigma_{cr}^N(i, j)$ indicating these stress changes. The values of $\sigma_{cr}^N(i, j)$ are set to 0 at the beginning of the earthquake (with index N) occurring at time t_N .

(a) Nearest neighbor interactions (NN model):¹

The stresses in the crust are assumed to increase in the positions of the four adjacent blocks:

$$\sigma_{cr}^N(k_{\pm}, l_{\pm}) \rightarrow \sigma_{cr}^N(k_{\pm}, l_{\pm}) + (0.25 - \alpha) \Delta\sigma \quad (7)$$

(b) Long-range interactions (LR model):

In this case, the stresses in the crust are assumed to increase spatially according to a Gaussian distribution:

$$\sigma_{cr}^N(i, j) \rightarrow \sigma_{cr}^N(i, j) + \frac{1-4\alpha}{\pi Q^2} e^{-\frac{(i-k)^2 + (j-l)^2}{Q^2}} \Delta\sigma \quad (8)$$

Instead of the Gaussian function, we could use alternatively the appropriate form to a perfectly elastic solid $1/r^3$ or an exponential screening function. However, the Gaussian function has the numerical advantage that it can be normalized and that it is spatially localized. Hence, finite size effects are less important and huge grid-sizes with high computational efforts can be avoided.

According to Eq. (5), the sliding of block (k, l) redefines the stresses $\sigma(k_{\pm}, l_{\pm})$ acting on the adjacent blocks. This may lead to an instability, i.e., $\sigma(k_{\pm}, l_{\pm}) \geq \sigma_F$, in one or more adjacent blocks. In this case, a chain reaction starts and the stresses are distributed according to Eqs. (5), (6), and (7), respectively (8), until the earthquake is terminated, i.e., until $\sigma(i, j) < \sigma_F$ for all blocks (i, j) . The spatial size S of the event is measured; that is, the blocks, which slipped at least once in the avalanche, are counted.

2. In the inter-occurrence time interval between successive events, the dynamics are described in the following way: The evolution of a single earthquake is set to be instantaneous; that is, the crust relaxation process and the tectonic loading have no effect during the evolution of an earthquake. After an earthquake occurring at time t_n , transient creep is assumed to lead to a stress increase

$$\Delta\sigma^n(i, j, t) = \kappa \sigma_{cr}^n(i, j) (1 - e^{-\frac{t-t_n}{T}}), \quad (9)$$

where the relaxation time T as well as κ are parameters of the model. The parameter κ denotes the fraction $0 < \kappa < 1$ of the instantaneous stress jump in the crust σ_{cr}^n , which is redistributed to the fault in time. A schematic plot of this temporal dependence is shown in Figure 2. The overall dynamics due to all relaxation processes, triggered by the earthquakes in the past, can be determined by superposition. Additionally to the crust relaxation process, the movement of the tectonic plates increases the stress on each block with a constant rate $(\sigma_F - \sigma_R)/T_0$, where T_0 is the tectonic reloading time. Therefore the time evolution of the stress distribution following an earthquake at time $t = t_N$ can be described

¹This case is called nonlocal model in (Hainzl et al., 1999).

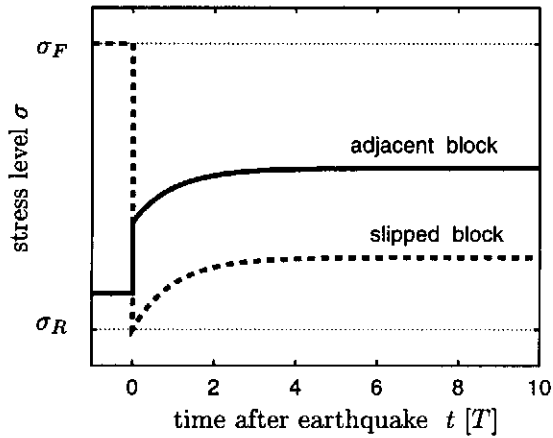


Fig. 2. The schematic plot illustrates the time-delayed stress changes subsequently to the instantaneous stress jumps due to an earthquake at time 0. At the occurrence time of the earthquake, the stress drops instantaneously at the slipped block and increases at adjacent blocks. As a result of the crust relaxation process with relaxation time T , the stresses increase after the earthquake on the four nearest neighbors (NN model), respectively, on the slipped block as well as on its extended neighborhood (LR model).

by

$$\begin{aligned} \sigma(i, j, t) &= \sigma(i, j, t_N) + \frac{\sigma_F - \sigma_R}{T_0} (t - t_N) \\ &+ \sum_{n=1}^N [\Delta\sigma^n(i, j, t) - \Delta\sigma^n(i, j, t_N)] \\ &= \sigma(i, j, t_N) + \frac{\sigma_F - \sigma_R}{T_0} (t - t_N) \\ &+ \kappa S_N(i, j) (1 - e^{-\frac{t-t_N}{T}}). \end{aligned} \quad (10)$$

The function $S_N(i, j)$ can be calculated iteratively by

$$\begin{aligned} S_N(i, j) &\equiv \sum_{n=1}^N \sigma_{cr}^n(i, j) e^{-\frac{t_N - t_n}{T}} \\ &= \sigma_{cr}^N(i, j) + S_{N-1}(i, j) e^{-\frac{t_N - t_{N-1}}{T}}, \end{aligned} \quad (11)$$

where t_n is the occurrence time of the n th event. To determine the onset of the following earthquake (index $N+1$), the equations $\sigma(i, j, \tilde{t}_{ij}) = \sigma_F$ are solved with Newton's method and the block with the minimal time $t_{\min} = \min\{\tilde{t}_{ij} | i, j \in 1, \dots, L\}$ is picked up. The next earthquake is initiated at this block and occurs at time $t_{N+1} = t_{\min}$. All stresses are changed to the values $\sigma(i, j, t_{\min})$ according to (10), and step 1 is repeated for the next earthquake.

3 Numerical simulations

For the numerical simulations, we use open boundary conditions and start with random values of $\sigma(i, j)$ uniformly distributed in the interval $[\sigma_R, \sigma_F]$. The values

of σ_R and σ_F have no influence on the dynamics. They are set arbitrarily to $\sigma_R=0$ and $\sigma_F=1$. Furthermore, the tectonic reloading time T_0 can be fixed arbitrarily, because it defines just the time scale. Therefore, apart from the system size $L \times L$, the parameters of our model are the elastic coupling constant α , the relative stress relaxation time T/T_0 , the feedback strength κ , and additionally in the case of long-range interactions, the spatial coupling length Q . The system is iterated until it reaches a statistically stationary state.

By setting $\kappa=0$, our model is equivalent to the OFC model. To illustrate the consequences of $\kappa \neq 0$; that is, the effect of the memory term in Eq. (10), an example of the seismic activity accompanying a large event is shown in Fig. 3 for both cases. The transient creep leads obviously to a clustering of smaller events in the temporal vicinity of the mainshock, whereas clustering is absent in the case of the OFC model. In the following sections, the simulations are analyzed in more detail. At first, we study the distribution of event sizes. In the second part, we investigate the spatio-temporal patterns

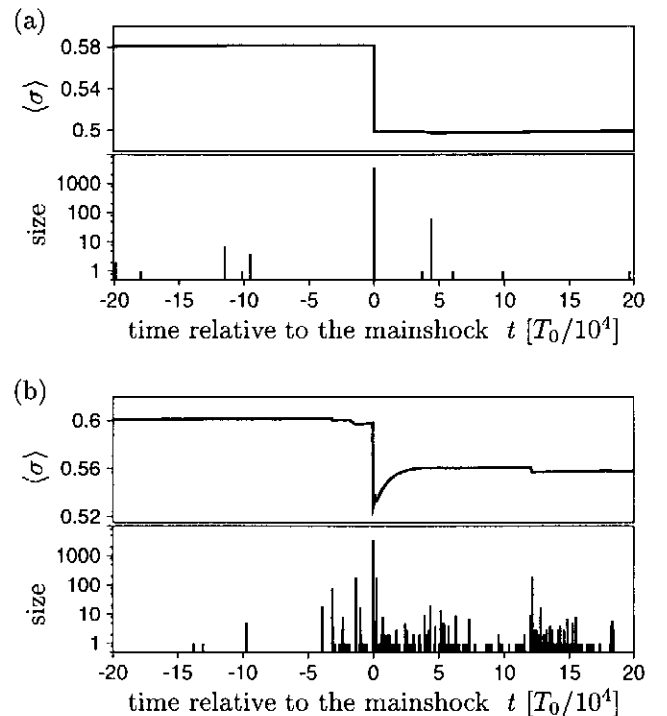


Fig. 3. The effect of transient creep is illustrated by means of typical examples of the seismic activity accompanying large events: (a) without the relaxation mechanism ($\kappa=0$, $\alpha=0.2$); that is, the OFC model; and (b) including the relaxation mechanism (NN model with $\kappa=0.5$, $\alpha=0.2$, and $T/T_0=10^{-4}$). For both 100×100 block simulations, the mean stress level $\langle \sigma \rangle = \sum \sigma(i, j) / L^2$ (upper curve) and the size of occurring events (bottom curve) are shown as a function of time. In the case of the extended model, the assumed transient characteristics are responsible for the partial stress recovery subsequent to earthquakes leading to a pronounced bunching of events in the vicinity of the largest earthquake. Note that transient creep occurs subsequently to all events, although the plotted curve $\langle \sigma \rangle(t)$ reflects this for the largest events only.

of the earthquake dynamics, in particular, we analyze the characteristics of foreshock and aftershock sequences as well as the waiting time distribution.

3.1 Frequency-size distribution

For the NN model, previous investigations (Hainzl et al., 1999) have shown that the model dynamics evolve independent of the initial conditions in a statistically stationary state which is characterized by a power law scaling of the size distribution, limited only by the finite system size. By analogy with the OFC model (Olami et al., 1992), the observed exponent B (Eq. 2) is significantly influenced only by the elastic parameter α and increases, if α decreases. Realistic values, $B \approx 1$, can be reproduced with $\alpha \approx 0.2$.

In the case of the long-range interactions, these characteristics are maintained. For the coupling constant $\alpha = 0.2$, Fig. 4 shows the distributions for different coupling length Q in comparison to that obtained using nearest neighbor interactions. No significant deviations are found.

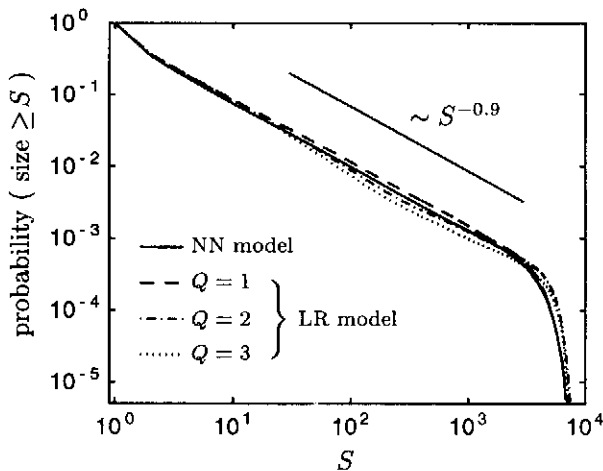


Fig. 4. Probability density of observing an earthquake of size greater than S as a function of S for the model with nearest neighbor, respectively long-range interactions. Each distribution results from a simulation of a 100×100 block-system with model parameters $T/T_0 = 10^{-4}$, $\alpha = 0.2$, and $\kappa = 0.5$.

In the following sections, we restrict our analysis to simulations with the parameter $\alpha = 0.2$ yielding a realistic Richter B value.

3.2 Foreshock and aftershock sequences

In this section, we analyze our model simulations with regard to spatio-temporal clusters accompanying mainshocks. A mainshock is defined as an event of size $S \geq S_{\text{cut}}$, which is the largest event within its temporal vicinity $\pm \Delta t_M$. For the analyzed 100×100 block simulations, we use the definitions $S_{\text{cut}} = 1000$ and $\Delta t_M = T_0/10$.

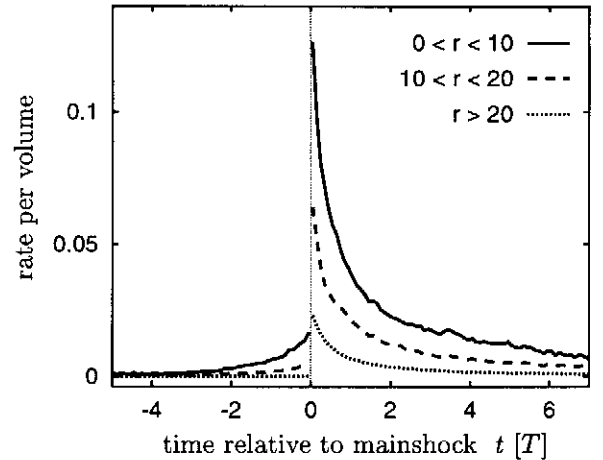


Fig. 5. Averaged earthquake occurrence rate per spatial volume formed by stacking the records of seismic rate relative to mainshock occurrence times. The rate depends on the distance r to the hypocenter of the mainshock. The curves show the average of the seismic rate regarding the 5000 mainshocks occurring in a 100×100 block simulation of about 10^7 earthquakes (NN model with $T/T_0 = 10^{-4}$, $\alpha = 0.2$, and $\kappa = 0.5$).

3.2.1 Rate of foreshocks and aftershocks

We compute the seismic activity, especially the rate of events, occurring on average relative to those mainshocks. For the NN model, Fig. 5 shows the averaged occurrence rate per spatial volume in dependence on the spatial distance r to the hypocenter (initiation point) of the mainshock. An increasing number of foreshocks is generated, on average, just before the mainshock. Aftershocks turn on instantaneously with the mainshock, followed by a decay of the aftershock rate. The rate of aftershocks exceeds the rate of foreshocks by about 1 order of magnitude. It is important to note that the number of foreshocks as well as the number of aftershocks decreases with increasing distance r from the hypocenter of the mainshock; that is, the clusters are localized around the hypocenter of the mainshock. These characteristics are not restricted to the case of nearest neighbor coupling, rather it is also observed in the case of spatially extended regions of transient creep (LR model).

In Fig. 6 the occurrence rates of events are shown in log-log plots for the NN model as well as for the LR model with $Q=1, 2$, and 3 . The relative relaxation time is set to $T/T_0 = 10^{-4}$ in all cases. The variations in each data set, namely the increase of foreshock as well as the decrease of aftershock activity, can be fitted quite well by, aside from a factor, identical modified Omori laws (Eq. 3, respectively 4). This is in good agreement with findings for real fault systems (Papazachos, 1975; Kagan and Knopoff, 1978; Jones and Molnar, 1979; Davis and Frohlich, 1991). In previous investigations of the NN model, we have found that the relative relaxation time T/T_0 determines the power law exponent (Hainzl

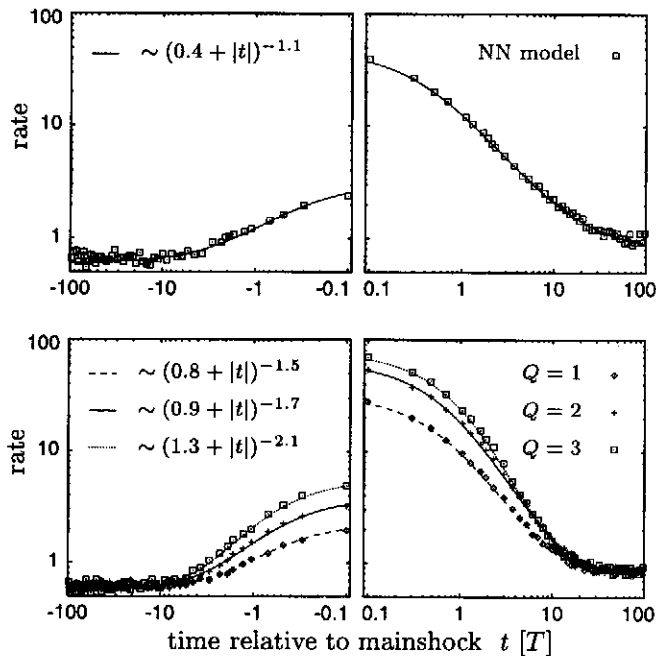


Fig. 6. Log-log plots of earthquake clustering formed by stacking the records of seismic activity relative to mainshock times. The plots show the average of event clustering corresponding to 5000 mainshocks of size $S \geq 1000$ occurring in 100×100 -grid model simulation with $T/T_0 = 10^{-4}$, $\alpha = 0.2$ and $\kappa = 0.5$. The results are shown for the NN model (upper plots), and the LR model with $Q=1, 2$, and 3 (bottom plots). For each data set the increase of foreshock activity (left column) as well as the decrease of aftershock activity (right column) can be fitted by similar power laws differing in a prefactor only.

et al., 1999). The exponent of the power law decreases approximately by 1.6, 1.1, and 0.6 for increasing ratio $T/T_0 = 10^{-5}$, 10^{-4} , and 10^{-3} , respectively. Thus the empirical values $p, q \approx 1$ can be reproduced in this case by a ratio T/T_0 of the order of 10^{-4} .

Here, we find that also the spatial extension of transient creep changes significantly the exponent: The larger Q the larger is the exponent. An explanation is that mainshocks occur when the block-system is critical loaded. The stress redistribution due to the mainshock unloads the system only partly remaining other parts of the block-system critical loaded. The subsequent stress increase owing to transient creep triggers aftershocks which trigger further aftershocks and so on, until the whole system is subcritical. In the case of long-range interactions, each event can trigger more subsequent events, thus the process decays faster.

Therefore in addition to different relaxation times, a variable spatial scale of transient creep can be responsible for the variation of empirically observed p values scattering between 0.9 and 1.5 (Utsu et al., 1995).

In summary, the main characteristics, in particular the power law distribution of event sizes and the occurrence of foreshock and aftershock sequences obeying the Omori law, are reproduced independently of the spa-

tial range of creep. Only in the unrealistic case that transient creep is restricted to the slipped blocks, the empirical observations cannot be reproduced (Hainzl et al., 1999). For the further investigations we use nearest neighbor instead of the long-range interactions, because of less computational efforts. The model parameters are set to $T/T_0 = 10^{-4}$ and $\alpha = 0.2$ leading to the empirically observed power law exponents B, p , and q .

3.2.2 Temporal variations of aftershock sizes

Up to now, we have analyzed only the temporal variations of the aftershock rate. Now, we want to characterize the aftershock size in dependence on the aftershock occurrence time relative to the mainshock. The sizes of aftershocks occurring subsequently to 1000 mainshocks are measured in time bins of $\Delta t = T$. Fig. 7 shows the temporal variation of the mean as well as of the maximum size of aftershocks occurring in these time bins, on average, after a mainshock. The mean aftershock size is almost independent of time, whereas the maximum size decreases with time from approximately 100 immediately after the mainshocks down to approximately 14. Therefore the maximum aftershock size is on average at least one order of magnitude less than the mainshock size. This is in good agreement with empirical findings (Scholz, 1994). The decrease of the maximum size is due to the fact that the rate of aftershocks decreases with time (see Fig. 6); thus the probability to observe larger aftershocks is higher in the vicinity of the mainshock, although the probability distribution for event sizes is almost stable.

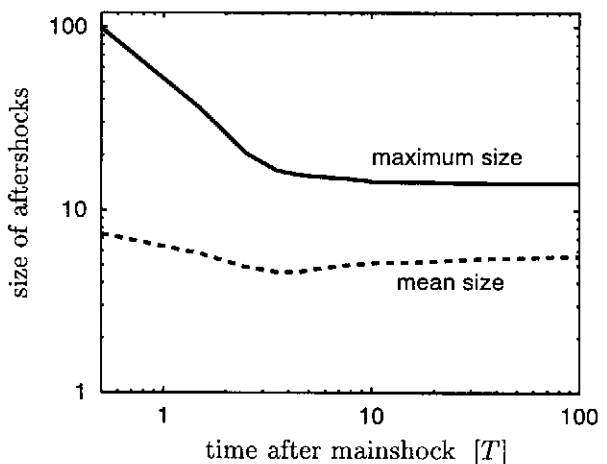


Fig. 7. The size of aftershocks in dependence on their occurrence times after the mainshock. The mean and the maximum aftershock size are computed by averaging over the 1000 mainshocks with size greater than 1000 which have occurred in a 100×100 -lattice simulation of about 2×10^6 events (NN model with $T/T_0 = 10^{-4}$, $\alpha = 0.2$, and $\kappa = 0.5$).

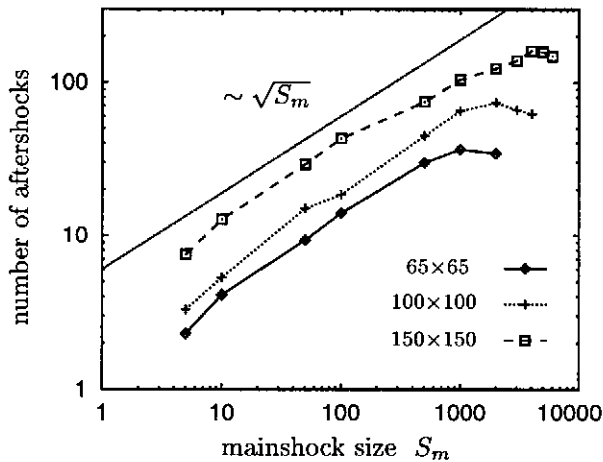


Fig. 8. The cumulative number of aftershocks occurring on average within $10 \times T$ after mainshocks of size S_m . The three curves, corresponding to different system sizes $L \times L$, are compared with the power law $\sim \sqrt{S_m}$. The analyzed simulations (NN model with $T/T_0 = 10^{-4}$, $\alpha = 0.2$, and $\kappa = 0.5$) consist in the case of $L = 65$, respectively 100, of 10^7 events and in the case of $L = 150$ of 2×10^6 events.

3.2.3 Cumulative number of aftershocks

The number of aftershocks depends on the size of the triggering mainshock. This is shown in Fig. 8. For that plot, we have counted all events occurring within the time window of $10 \times T$ subsequently to mainshocks of size S_m . Here, we have used a slightly different definition for a mainshock of size S_m , namely, it is defined as an event of size $S \in [S_m - S_m/10, S_m + S_m/10]$, which is the largest event within a time interval $\pm 10 \times T$.

The characteristics of all three curves, corresponding to different lattice sizes, are the same: The number of aftershocks increases almost according to a power law $\sim S_m^{0.5}$, limited only by the finite system size. The finite size effect manifests itself in the deviation from power law behavior observed for the largest mainshocks. However, the larger the lattice size, the later occurs this deviation. In agreement with our results, a power law increase can also be fitted to the cumulative number of real aftershocks, although approximations of the exponent vary largely, mainly between 0.3 and 1 (Reasenber, 1985; Guo and Ogata, 1997). The exponent of nearly 0.5, which is found in our model simulations, indicates that aftershocks are triggered mostly on the edge of the fracture area of the mainshock. In the case of a circular fracture area S_m , the edge is proportional to the radius, i.e. proportional to $\sqrt{S_m}$.

3.3 Distribution of waiting times

To study the overall characteristics of temporal clustering in our model simulation, we analyze the distribution of waiting times t_w ; that is, the inter-occurrence time intervals between successive events. This distribution is

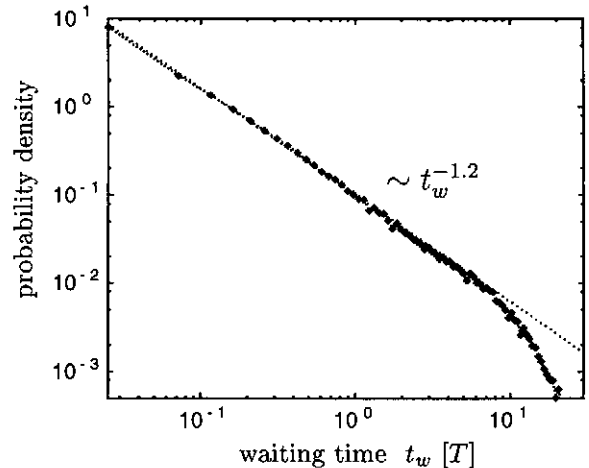


Fig. 9. The probability density of observing a waiting time t_w between two successive events. The plot results from a simulation of 10^6 events (NN model with $T/T_0 = 10^{-4}$, $\alpha = 0.2$, $\kappa = 0.5$, and $L = 100$). The dotted line indicates the power law $t_w^{-1.2}$.

shown in Fig. 9 for a simulation of the NN model with a relative relaxation time $T/T_0 = 10^{-4}$. The distribution can be fitted over almost three orders of magnitude by a power law with exponent -1.2. This power law behavior is in good agreement with empirical observations (Ito, 1995; Utsu et al., 1995). However, this is not surprising owing to the power law behavior of aftershock sequences. Senshu (1959) showed that if the aftershocks are represented by a non-stationary Poisson process whose intensity is proportional to t^{-p} , a power law distribution $t_w^{-p_w}$ of waiting times is derived directly and the relation between p and p_w should be

$$p_w = 2 - p^{-1}. \quad (12)$$

In our model, simulations with $T/T_0 = 10^{-4}$ lead to an exponent $p \approx 1.1$ of the modified Omori law (Eq. 3). Thus Eq. (12) is nearly fulfilled for our deterministic model, although the exponent of the waiting time distribution p_w is obtained in this case for the whole sequence including all events belonging to the background activity.

In the following part, we want to characterize the waiting time distribution, if events greater than a minimal size S_{cut} are considered only. A suitable measure to characterize the waiting time distribution is the coefficient of variation C_V , which is defined as the standard deviation normalized by the mean waiting time (t_w) (Kagan and Jackson, 1991)

$$C_V = \frac{\sqrt{\langle (t_w)^2 \rangle - \langle t_w \rangle^2}}{\langle t_w \rangle}. \quad (13)$$

For a simple periodic signal C_V vanishes, whereas for a Poisson process the distribution function of the waiting times is an exponential function yielding $C_V = 1$. A clustering of events is indicated by $C_V > 1$.

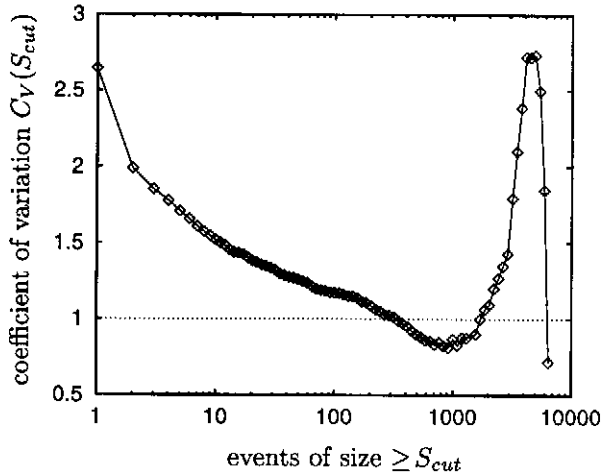


Fig. 10. The coefficient of variation C_V (Eq. 13), calculated for all events greater than S_{cut} , as a function of the lower cut. The result is shown for the same simulation analyzed in Fig. 9. Small and large earthquakes are characterized by a coefficient greater than 1, implying earthquake bunching.

We compute the coefficient of variation for the simulation analyzed in Fig. 9. Now, we consider only earthquakes with a size greater than S_{cut} . Figure 10 shows the value of C_V in dependence on this lower cut. The coefficient C_V is greater than 1 for small and large values of S_{cut} , implying earthquake clustering. The decrease for very large earthquakes is a finite size effect and thus related to the cutoff in the frequency-size distribution (Fig. 4). For intermediate values of S_{cut} , the earthquake occurrence seem to be uncorrelated.

Clustering for small values of S_{cut} can be explained by foreshock and aftershock sequences triggered by transient creep. These clusters consist mainly of smaller events (see Fig. 7). Thus increasing of S_{cut} leads to partial deletion of these sequences and consequently to a decrease of C_V .

In contrast, large events are correlated in time because they are correlated in space. This correlation emerges because of dissipation ($\alpha < 0.25$ and $\kappa < 1$). This is already known for the nonconservative, cellular automaton versions of the BK model; that is, for our model with $\kappa = 0$. In this case, Rundle and Klein (1995) found strong correlations between the spatial fracture areas of subsequent large earthquakes and Christensen and Olami (1992) observed, in analogy to our results with $\kappa \neq 0$, temporal clustering of large events. For the case of $\kappa = 0.5$, Fig. 11 shows an example of large events occurring subsequently in a simulation of the NN model. They are obviously bunched, which is in good agreement with observations of the occurrence of large earthquakes in nature (Kagan and Jackson, 1991). These clustering characteristics are found to be independent of the assumed spatial extension of transient creep, namely they are observed also in the LR model.

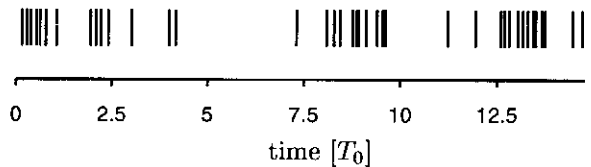


Fig. 11. An example of temporal occurrence of successive large events ($S > 3000$) in the NN model.

4 Summary and conclusion

It was known before that nonconservative, cellular automaton versions of the BK model can reproduce the empirically observed power law behavior of the frequency-size distribution of earthquakes. However, they have failed to reproduce the most conspicuous characteristics of spatio-temporal clustering observed in real fault systems, namely the occurrence of foreshock and aftershock sequences accompanying large earthquakes as well as the occurrence of swarms of small events. We have shown that this inability can be redressed by considering transient creep, which is observed to occur subsequently to earthquakes in real fault systems. In a first order approximation we have modeled the characteristics of transient creep by an exponential function decay in time and nearest neighbor as well as long-range effects in space. The model reproduces independently of the parameters and the spatial range of transient creep (as long as the effect of transient creep is not restricted to the slipped blocks) the most obvious characteristics manifested in real earthquake catalogs: (a) the distribution of earthquake sizes fulfills a power law (Gutenberg-Richter law), (b) the temporal increase of foreshock as well as the decrease of aftershock activity is characterized by similar power laws (modified Omori law), (c) foreshocks and aftershocks are spatially localized in the vicinity of the mainshock, (d) much more aftershocks than foreshocks occur, (e) the size of the largest aftershock is on average at least one order of magnitude less than the mainshock size, (f) the number of aftershocks increasing with the mainshock size according to a power law, and (g) small as well as large events are more likely to occur clustered than random. In further agreement with observations, we have shown in a previous work (Hainzl et al., 1999) that (h) the simulated foreshocks are characterized by a significant smaller Richter B value in comparison to aftershocks, or other events, and that (i) swarm events occur.

While the choice of model parameters does not change these characteristics in principle, the exponents of the frequency-size distribution B as well as of the Omori law p is found to dependent on this choice: The B value is determined mainly by the coupling constant α , whereas the relative relaxation time T/T_0 as well as the spatial scale Q of transient creep change the p value. On the other hand the parameter characterizing the strength of

transient creep κ and the spatial size of the system L do not influence any of the power law exponents significantly. However, the number of foreshocks and aftershocks occurring in the simulations are positively correlated with κ and L (Hainzl et al., 1999).

In summary, we have shown that block systems, involving nothing else than elastic interactions with an exponentially decaying memory in addition, self-organize into a statistically stationary state with striking similarities to empirical observations. In spite of the fact that the actual dynamical processes involved in earthquake faults are much more complicated, we believe that our conceptual model bears a strong resemblance to the mechanisms most important for the underlying dynamics of earthquakes.

Acknowledgements. The authors are grateful to R. Engbert, F. Scherbaum, and J. Zschau for stimulating discussions. This work was supported by the Sonderforschungsbereich 555 "Komplexe Nichtlineare Prozesse" and the state Brandenburg (Hochschulsonderprogramm III 1.6).

References

- Bak, P., and Tang, C., Earthquakes as a self-organized critical phenomenon, *J. Geophys. Res.*, *94*, 15635–15637, 1989.
- Bak, P., Tang, C., and Wiesenfeld K., Self-organized criticality: An explanation of $1/f$ noise, *Phys. Rev. Lett.*, *59*, 381–384, 1987.
- Brown, S. R., Scholz, C. H., and Rundle, J. B., A simplified spring-block model of earthquakes, *Geophys. Res. Lett.*, *18*, 215–218, 1991.
- Burridge, R., and Knopoff, L., Model and theoretical seismicity, *Bull. Seis. Soc. Am.*, *57*, 341–371, 1967.
- Carlson, J. M., and Langer, J. S., Properties of earthquakes generated by fault dynamics, *Phys. Rev. Lett.*, *62*, 2632–2635, 1989a.
- Carlson, J. M., and Langer, J. S., A mechanical model of an earthquake fault, *Phys. Rev. A*, *40*, 6470–6484, 1989b.
- Christensen, K., and Olami, Z., Variation of the Gutenberg-Richter b-values and nontrivial temporal correlations in a spring-block model for earthquakes, *J. Geophys. Res.*, *97*, 8729–8735, 1992.
- Davis, S. D., and Fröhlich, C., Single-link cluster analysis of earthquake aftershocks: Decay laws and regional variations, *J. Geophys. Res.*, *96*, 6335–6350, 1991.
- DeMets, C., Afterslip no longer an afterthought, *Nature*, *386*, 549, 1997.
- Dieterich, J. H., Time-dependent friction as a possible mechanism for aftershocks, *J. Geophys. Res.*, *77*, 3771–3781, 1972.
- Ekström, G., and Dziewonski, A. M., Evidence of bias in estimations of earthquake size, *Nature*, *332*, 319–323, 1988.
- Guo, Z., and Ogata, Y., Statistical relations between the parameters of aftershocks in time, space, and magnitude, *J. Geophys. Res.*, *102*, 2857–2873, 1997.
- Gutenberg, B., and Richter, C. F., Earthquake magnitude, intensity, energy and acceleration, *Bull. Seismol. Soc. Am.*, *46*, 105–145, 1954.
- Hainzl, S., Zöller, G., and Kurths, J., Similar power laws for foreshock and aftershock sequences in a spring block model for earthquakes, *J. Geophys. Res.*, *104*, 7243–7253, 1999.
- Heki, K., Miyazaki, S., and Tsuji, H., Silent fault slip following an interplate thrust earthquake at the Japan Trench, *Nature*, *386*, 595–598, 1997.
- Ito, K., Punctuated-equilibrium model of biological evolution is also a self-organized-criticality model of earthquakes, *Phys. Rev. E*, *52*, 3232–3233, 1995.
- Ito, K., and Matsuzaki, M., Earthquakes as self-organized critical phenomena, *J. Geophys. Res.*, *95*, 6853–6860, 1990.
- Jones, L. M., and Molnar, P., Some characteristics of foreshocks and their possible relationship to earthquake prediction and premonitory slip on faults, *J. Geophys. Res.*, *84*, 3596–3608, 1979.
- Kagan, Y. Y., and Jackson, D. D., Long-term earthquake clustering, *Geophys. J. Int.*, *104*, 117–133, 1991.
- Kagan, Y. Y., and Knopoff, L., Statistical study of the occurrence of shallow earthquakes, *Geophys. J. R. Astron. Soc.*, *55*, 67–86, 1978.
- Kanamori, H., and Anderson, D. L., Theoretical basis of some empirical relations in seismology, *Bull. Seis. Soc. Am.*, *65*, 1073–1095, 1975.
- Nakanishi, H., Cellular-automaton model of earthquakes with deterministic dynamics, *Phys. Rev. A*, *41*, 7086–7089, 1990.
- Olami, Z., Feder, H. S., and Christensen, K., Self-organized criticality in a continuous, nonconservative cellular automaton modeling earthquakes, *Phys. Rev. Lett.*, *68*, 1244–1247, 1992.
- Omori, F., On the aftershocks of earthquakes, *J. Coll. Sci. Imp. Univ. Tokyo*, *7*, 111–200, 1894.
- Pacheco, J. F., Scholz, C. H., and Sykes, L. R., Changes from frequency-size relationship from small to large earthquakes, *Nature*, *355*, 71–73, 1992.
- Papazachos, B. C., Foreshocks and earthquake prediction, *Tectonophysics*, *28*, 213–226, 1975.
- Peltzer, G., Rosen, P., Rogez, F., and Hudnut, K., Postseismic rebound in fault step-overs caused by pore fluid flow, *Science*, *273*, 1202–1204, 1996.
- Purcaru, G., and Berckhemer, H., A magnitude scale for very large earthquakes, *Tectonophysics*, *49*, 189–198, 1978.
- Reasenberg, P., Second-order moment of Central California seismicity, 1969–1982, *J. Geophys. Res.*, *90*, 5479–5495, 1985.
- Rundle, J. B., and Klein, W., Dynamical segmentation and rupture patterns in a toy slider-block model for earthquakes, *Nonlin. Proc. Geophys.*, *2*, 61–79, 1995.
- Savage, J. C., and Svarc, J. L., Postseismic deformation associated with the 1992 $M_w=7.3$ Landers earthquake, southern California, *J. Geophys. Res.*, *102*, 7565–7577, 1997.
- Scholz, C. H., *The Mechanics of Earthquakes and Faulting*, Cambridge University Press, 1994.
- Senshu, T., On the time interval distribution of aftershocks, *Zisin, Ser. 2*, *12*, 149–161, 1959 (in Japanese).
- Utsu, T., Ogata, Y., and Matsu'ura, R. S., The centenary of the Omori formula for a decay law of aftershock activity, *J. Phys. Earth*, *43*, 1–33, 1995.